Influences of Element Types on Nonlinear Finite Element Analysis of a Concrete Column Under Near-Field Blast Loading

Xu, Jie; Hendriks, Max A.N.; Rots, Jan G.; Tsouvalas, Apostolos

DOI
10.1007/978-981-99-2375-5_31

Publication date
2023

Document Version
Final published version

Published in
Recent Advances in Applied Mechanics and Mechanical Engineering

Citation (APA)
Xu, J., Hendriks, M. A. N., Rots, J. G., & Tsouvalas, A. (2023). Influences of Element Types on Nonlinear Finite Element Analysis of a Concrete Column Under Near-Field Blast Loading. In S. Yadav, H. Kumar, M. Wan, P. K. Arora, & Y. Yusof (Eds.), *Recent Advances in Applied Mechanics and Mechanical Engineering: Select Proceedings of ICAMME 2022* (pp. 311-321). (Lecture Notes in Mechanical Engineering). Springer. https://doi.org/10.1007/978-981-99-2375-5_31

Influences of Element Types on Nonlinear Finite Element Analysis of a Concrete Column Under Near-Field Blast Loading

Jie Xu, Max A. N. Hendriks, Jan G. Rots, and Apostolos Tsouvalas

Abstract Due to the accompanying severe consequences of explosions, the blast puts a great threat to public security. Nonlinear finite element analysis is a possible method for civil engineers to check the integrity of the structures under blast loading without underestimating the limit of the structures. However, different choices of element types would generally put a great influence on the analytical results and the corresponding computational expenses. Therefore, how should civil engineers simplify their physical model into finite element models to gain relatively accurate numerical results with acceptable computational expenses is of great interest. In this article, 6 different types of elements are discussed with different orders and shapes for a certain physical situation, and the corresponding experimental results and the numerical results for a very detailed finite element model are used as the baseline for judgement, which could be helpful for civil engineers to make proper simplifications in the set-up of finite element models.

Keywords Nonlinear finite element analysis · Blast · Solution strategy

1 Introduction

Explosions, having a low probability of occurrence in daily life, the accompanying consequences are extremely severe in most cases due to the potential collapse of structures, are known as "Low Probability and High Consequences (LP-HC)" events.

J. Xu (✉)
College of Aerospace Science and Engineering, National University of Defense Technology, Changsha 410073, Hunan, China
e-mail: vitavitavitalopez@icloud.com

Hunan Key Laboratory of Intelligent Planning and Simulation for Aerospace Missions, Changsha 410073, Hunan, China

M. A. N. Hendriks · J. G. Rots · A. Tsouvalas
Faculty of Civil Engineering and Geosciences, Delft University of Technology, Delft, Zuid Holland 2628 CN, The Netherlands

S. Yadav et al. (eds.), *Recent Advances in Applied Mechanics and Mechanical Engineering*, Lecture Notes in Mechanical Engineering,
https://doi.org/10.1007/978-981-99-2375-5_31

Not only the accidental explosion, but also the premeditated attack puts a great threat to public security [1]. For this reason, it could be of great necessity for civil engineers to take the structural integrity of structures under blast loading into consideration during the design process.

Nonlinear finite element analysis is a potentially helpful tool for civil engineers to predict structural integrity without underestimation of the capacities of structures. However, before the set-up of the nonlinear finite element models, different civil engineers would have different choices in the element types, which would lead to considerable differences in the numerical results and the corresponding computational expenses.

For nonlinear finite element analysis of reinforced concrete structures under blast loading, Toy et al. did a series of experiments and numerical analyses for reinforced concrete slabs and reinforced concrete retaining walls [2–4]. Most of the comparisons between the analytical results and the experimental observations focused on the deformed shapes and cracking patterns.

Siba did 16 experiments on reinforced concrete columns with different reinforcement detailings and different stand-off distances. During the experiments, pressure gauges and string potentiometers were used to record the blast pressure–time histories and displacement–time curves [5].

Existing methods for predicting blast loading on a structure are generally based on the analytical work of Brode [6] or the Kingery/Kingery and Bulmash semi-empirical relations [7, 8], which is widely used in commercial finite element analysis software like LS-DYNA and ABAQUS. These methods are accurate for simple scenarios with spherical or semi-spherical explosives under free-air bursts. Nevertheless, cylinders are known as one of the most common shapes of explosives. Jordan et al. did a series of research on the blast shock wave generated by cylindrical charge, and it has been certificated that the characteristics of the stress distribution and wave propagation of cylindrical explosives are very different from spherical explosives [9–12].

Based on Siba's experiments, 6 finite element models are established with different element types and orders, and 5 groups are divided to make the comparison between the analytical results.

2 Experiments

The column named CONV-7 from Siba's experiments is selected as the baseline of comparison. Figure 1 presents the set-up of the experiment. Two columns were tested in pairs, and a 100 kg cylindrical ANFO with 1.30 m height was denotated to create the shockwave.

Pressure gauges were attached to both the front and the rear surfaces of the column to record the blast pressure–time diagrams and string potentiometers were attached to the rear surface of the column to record the displacement–time curves. Figure 2 demonstrates the detailed locations of pressure gauges and string potentiometers.

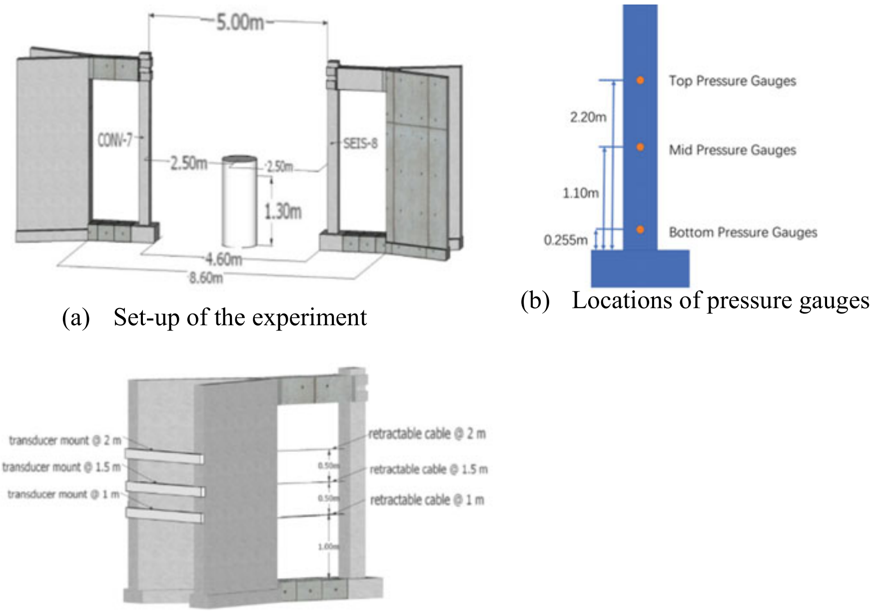

(a) Set-up of the experiment

(b) Locations of pressure gauges

(c) Locations of string potentiometers

Fig. 1 Set-up of the experiment [5]

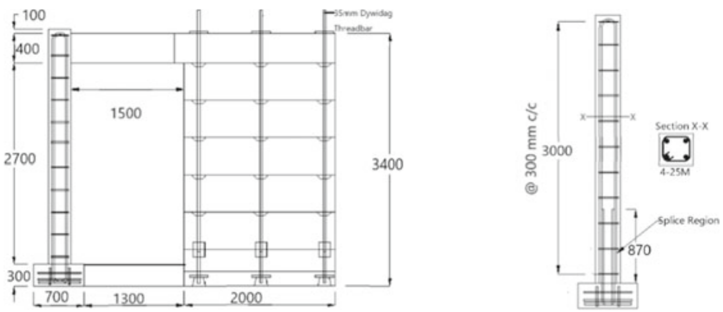

(a) Geometric information of column CONV-7

(b) Reinforcement detailings

Fig. 2 Detailed information of the column CONV-7 for modelling set-up [5]

C35 was used for the column and C70 was used for the support structures. Tensile tests were executed for the reinforcement rebars, which give detailed information about the mechanical properties of the rebars. 10 M rebars with 11.3 mm diameter were used as the ties, and 25 M rebars with 19.5 mm diameter were used as the longitudinal rebars. Pre-tensioned DYWIDAG Threadbars were used in the support structures with 35 mm diameter. Detailed information about the reinforcements and

Table 1 Material properties of reinforcements [5]

Rebar size	Yield strength (MPa)	Yield strain	Ultimate strength (MPa)	Ultimate strain
10 M	465.2	0.0022	731.1	0.11
25 M	474.7	0.0024	673.2	0.11

geometries of the columns and the support structures is illustrated in Fig. 2 as well. The mechanical properties of 10 M rebars and 25 M rebars are listed in Table 1.

3 Modelling Set-up

DIANA FEA is applied in this article to perform the nonlinear finite element analysis as it could help to unify the iteration scheme and the convergence criteria, which could help to eliminate the influences of the solution strategies on the numerical results. At the same time, the CPU occupation could be recorded during the nonlinear finite element analysis, which helps to make a detailed comparison of the computational expenses.

3.1 Simplifications of Blast Loads

The negative phase of the explosive pressure–time history is usually not taken into consideration for the design purpose as it has been verified that the main structural damage is connected to the positive phase [13].

The simplification of the blast pressure–time diagrams is based on the assumption that a cylindrical explosive could be regarded as a combination of a set of small spherical explosives. With the recorded blast pressure–time diagrams, the blast pressure profiles could be interpolated. The peak overpressure value distribution of the front surface is assumed to be uniform within the lower 1.30 m of the surface, and Hopkinson-Cranz scaling law [14] is applied to interpolate the distribution of the upper front surface of the column. For the rear surface of the column, there are limited theories for the peak value distribution, and therefore, curve-fitting is used to interpolate the distribution of the peak overpressure. Figure 3 demonstrates the distribution of the peak overpressure among the front and rear surfaces of the column.

Due to the limitation of the DIANA FEA, the time-dependent factors of the front and rear surfaces could not be set as a function of the height. Therefore, uniform time-dependent factors are applied for both the front and rear surfaces [15]. Figure 4 presents the time-dependent factors of the front and rear surfaces, respectively. The rate-dependent factor is considered for the material model of concrete to take the strain-rate dependency into consideration, and based on Sluys' report, the rate-dependent factor is assumed to be 0.1 [16].

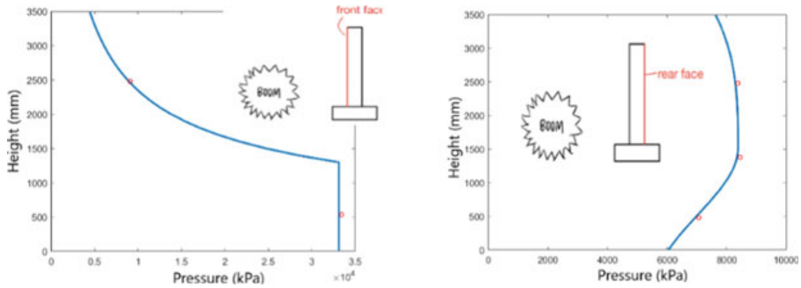

(a) Distribution of the peak pressure of the front surface

(b) Distribution of the peak pressure over the rear surface

Fig. 3 Interpolated peak pressure distributions

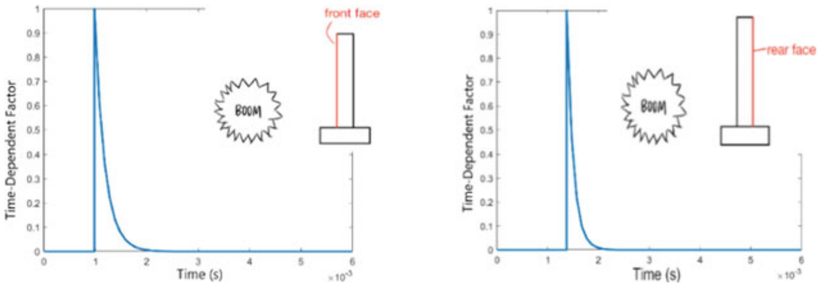

(a) Time-dependent factors of the front surface

(b) Time-dependent factors of the rear surface

Fig. 4 Time-dependent factors

3.2 Modelling Set-up

In this article, 6 finite element models are established and divided into 5 groups. Detailed information on the finite element models is listed in Table 2. And the detailed information for the group designation is given in Table 3. Due to the inclusion of the nonlinearity, with rapid change in loadings, there are difficulties in reaching convergence, therefore, different iteration schemes must be adopted for different models. The iteration schemes and convergence criteria are listed in Table 4.

For the 6 finite element models, the interpretation of the boundary conditions is demonstrated in Fig. 5a, and the bond-slip effect between the concrete and the rebars are not considered. For the detailed finite element model, based on which the comparison is made, the support structure is included and the boundary conditions are demonstrated in Fig. 5b, the bond-slip effect is included at the same time.

Table 2 Model designation

Model designation	Element type	Element Order	Mesh size (mm)
1	Solid	Linear	100
2	Plane stress	Linear	100
3	Beam	Linear	100
4	Solid	Quadratic	100
5	Plane stress	Quadratic	100
6	Beam	Quadratic	100

Table 3 Group designation

Group designation	Models
1	Model 1 & 2 & 3
2	Model 4 & 5 & 6
3	Model 1 & 4
4	Model 2 & 5
5	Model 3 and 6

Table 4 Iteration schemes and convergence criteria

Model	Self weight	Iteration method	Convergence criteria	Time steps	Iteration method	Convergence Criteria
1	1 step	RTNR[a]	Displ.:0.01 Force:0.01	0.05 ms 600 steps	MLNR[b]	Displ.:0.01
2	1 step	RTNR[a]	Displ:0.01 Force:0.01	0.05 ms 600 steps	MLNR[b]	Displ.:0.01
3	1 step	RTNR[a]	Displ:0.01 Force:0.01	0.05 ms 600 steps	MLNR[b]	Displ.:0.01
4	1 step	RTNR[a]	Displ:0.01 Force:0.01	0.05 ms 600 steps	MLNR[b]	Displ.:0.01
5	1 step	RTNR[a]	Displ:0.01 Force:0.01	0.05 ms 600 steps	MLNR[b]	Displ.:0.01
6	1 step	RTNR[a]	Displ:0.01 Force:0.01	0.05 ms 600 steps	RTNR[a]	Displ.:0.01

[a]Notes refers to the regular tangential Newton–Raphson iteration method
[b]Notes refers to the modified linear Newton–Raphson iteration method

However, for the detailed model, there is difficulty in reaching convergence, therefore, a combination of the iteration scheme is made. The information for the detailed finite element model is listed in Table 5.

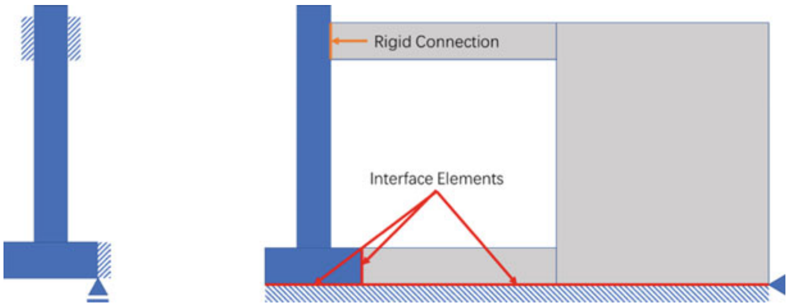

(a) Boundary conditions for the 6 finite element models

(b) Boundary conditions for the detailed model

Fig. 5 Interpretations of boundary conditions

Table 5 Information on the detailed finite element model

	Self-weight	Post-tension	Time steps		
	1 step	1 step	0.045 ms 2 steps	0.05 ms 60 steps	0.05 ms 522 steps
Iteration method	RTNR	RTNR	MLNR	RTNR	MLNR
Convergence criteria	Displ.:0.01 Force:0.01	Displ.:0.01 Force:0.01	Displ.:0.01	Displ.:0.01	Displ.:0.01

4 Results and Discussion

The numerical results of the 6 finite element models are summarized in Table 6. The first 30 ms after the detonation of the explosive are focused and the largest deformation of the point that locates on the rear surface of the column and 1.0 m away from the footing is compared. The maximum stresses and maximum crack widths are compared as well. The numerical results are given in Table 7.

Table 6 Summary of the numerical results

Model	1st natural Freq. (Hz)	2nd natural Freq. (Hz)	CPU	Largest Def. (mm)	Largest Def. at 1.0 m (mm)	Error (%)
1	97.498	102.52	747.28	22.51	18.8857	21.31
2	97.928	167.20	351.03	23.20	19.7247	17.814
3	114.26	149.75	289.33	23.26	18.6758	22.184
4	95.686	99.906	2272.42	24.69	21.3419	11.075
5	95.958	149.71	411.48	23.4	18.2059	24.142
6	97.498	161.43	355.17	26.16	22.6104	5.79
Detailed	72.210	89.438	4259.95	20.50	16.9420	29.408

Table 7 Summary of maximum stresses and crack widths

Model	Maximum stress (MPa)	Maximum crack width (mm)
1	492.57	1.60
2	494.69	2.31
3	493.44	1.31
4	540.06	2.86
5	552.17	2.76
6	521.39	4.35
Detailed	484.57	1.40

The displacement–time diagrams are presented in groups in Fig. 6. The curve in deep blue represents the recorded displacement–time curves during the experiment. And the computational expenses are illustrated in Fig. 7.

Based on the numerical results of Group 1 and Group 2, it could be observed that the finite element models with beam elements have the highest natural frequencies, which is the reason the translational constraints on models with beam elements are applied at the central axis of the column which restraint the rotations of the columns and the footings in a degree and therefore, introduce higher stiffness into the finite element models.

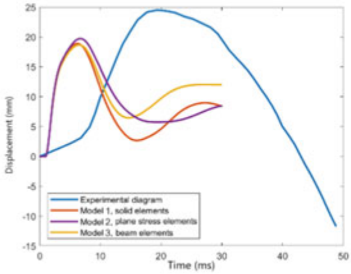

(a) Displacement-time diagrams of Group 1

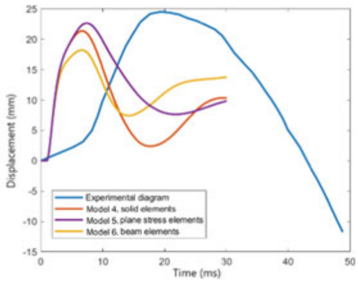

(b) Displacement-time diagrams of Group 2

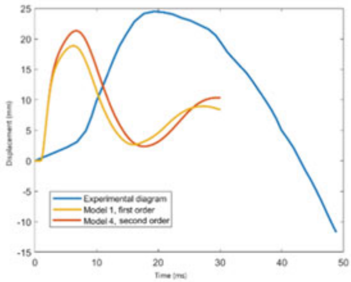

(c) Displacement-time diagrams of Group 3

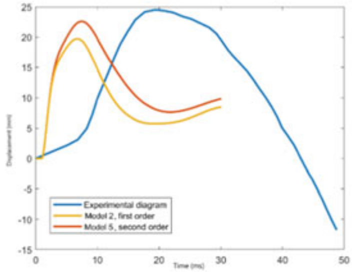

(d) Displacement-time diagrams of Group 4

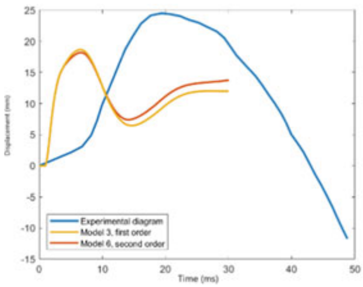

(e) Displacment-time diagrams of Group 5

Fig. 6 Displacement–time diagrams

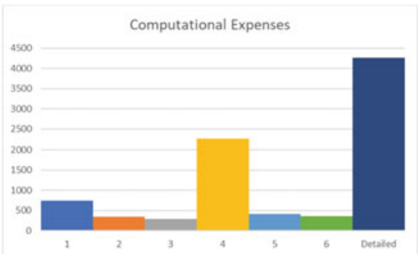

(a) Computational expenses

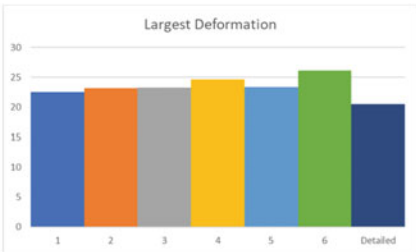

(b) Largest Deformation

Fig. 7 Differences in numerical results

5 Conclusion

The choice of dimensions and orders of elements shows a great influence on the numerical results and the corresponding computational efforts.

First-order elements are more recommended for nonlinear finite element analysis of structures under dynamic loadings due to the uniform mass distributions that would introduce fewer model uncertainties.

Plane stress elements are recommended at the preliminary design stage, which is extremely helpful in lowering the computational expenses and would generally yield conservative results with acceptable accuracies.

For models with beam elements, modifications of boundary conditions are required to ensure the rotations of the models would not be over-restricted.

Rayleigh damping coefficients based on the 1st and 2nd natural frequencies of finite element models are not proper enough for the structures under blast loading. For structures under blast loading, the loads should be considered as dynamic loads with extremely short periods, rather than impact, therefore, higher-order natural frequencies should be applied for the calculation of damping coefficients.

Further studies on solution strategies of nonlinear finite element analysis of structures under near-field explosions could focus on the calculation of the damping coefficients and the influence of the simplification of the blast pressure–time histories to help civil engineers gain more accurate numerical results on the displacement–time diagrams.

References

1. Olmati P, Petrini F, Bontempi F (2013) Numerical analyses for the structural assessment of steel buildings under explosions. Struct Eng Mech 45(6):803–819
2. Toy AT, Sevim B (2017) Numerically and empirically determination of blasting response of a RC retaining wall under TNT explosive. Adv Concr Constr 5:493–512
3. Wang F, Wan YKM, Chong OYK, Lim CH, Lim ETM (2008) Reinforced concrete slab subjected to close-in explosion. In: LS-DYNA Anwenderforum, pp 21–28
4. Carey NL, Myers JJ, Asprone D, Menna C, Prota A (2018) Polyurea coated and plane reinforced concrete panel behavior under blast loading: numerical simulation to experimental results. Trends Civ Eng Archit 1(4):87–98
5. Braimah A, Siba F (2017) Near-field explosion effects on reinforced concrete columns: an experimental investigation. Can J Civ Eng 45(4):289–303
6. Brode HL (1955) Numerical solutions of spherical blast waves. J Appl Phys 26(6):766–776
7. Kingery CN (1966) Air blast parameters versus distance for hemispherical TNT surface burst. Army Ballistic Research Lab Aberdeen Proving Ground MD
8. Kingery CN, Bulmash G (1984) Airblast parameters from TNT spherical air burst and hemispherical surface burst. US Army Armament and Development Center, Ballistic Research Laboratory
9. Jordan DW (1962) The stress wave from a finite, cylindrical explosive source. J Math Mech 503–551
10. Price MA (2005) Effects of cylindrical charge geometry and secondary combustion reactions on the internal blast loading of reinforced concrete structures (No. LA-14209-T). Los Alamos National Lab. (LANL), Los Alamos, NM (United States)

11. Knock C, Davies N (2013) Blast waves from cylindrical charges. Shock Waves 23(4):337–343
12. Rigby SE, Osborne C, Langdon GS, Cooke SB, Pope DJ (2021) Spherical equivalence of cylindrical explosives: effect of charge shape on deflection of blast-loaded plates. Int J Impact Eng 155:103892
13. Karlos V, Solomos G (2013) Calculation of blast loads for application to structural components. Publication Office of the European Union, Luxembourg
14. Hopkinson B, Cranz C (1915) Cube root scaling law
15. Diana FEA BV. Diana finite element analysis user's manual. https://dianafea.com/manuals/d102/Analys/Analys.html. Last Accessed 15 Sep 2022
16. Sluys LJ, de Borst R, Mühlhaus H-B (1993) Wave propagation, localization an dispersion in a gradient-dependent medium. Int J Solids Struct 30(9):1153–1171